Simulation of Piezo-Electric Injection for Gasoline DI Engines

P. Béard, O. Laget
IFP

ABSTRACT

The drive for substantial CO_2 reductions in gasoline engines in the light of the Kyoto Protocol and higher fuel efficiencies has increased research into Gasoline Direct Injection (GDI) engines. Moreover, using recently developed piezo-electric injection, stratified combustion can be achieved. This make possible combustion with low global fuel/air equivalence ratio which allows both a fuel saving and a decrease of pollutant emissions. The challenge for this type of DI engines is to control the fuel/air equivalence ratio in the area of the spark plug in order to get a good combustion. Optimal geometry design including appropriate piston and bowl shapes are required. The challenge for the numerical models is to have a very good representation of the spray and all the phenomena (as break-up or evaporation) occurring during and after the injection.

A model was developed to simulate piezo-electric injection. The transient opening and closing phases are taken into account. Comparisons between numerical results and experimental measurements of spray characteristics in a high pressure cell are shown for both non-evaporating and evaporating conditions. Then, results are shown for a direct injection spark ignition (DISI) engine. In all the studied configurations, results are in good agreement with the experimental measurements.

INTRODUCTION

Gasoline Direct Injection (GDI) engines bring benefits in terms of fuel efficiency by avoiding cross-flow. The challenge for this type of DI engines is to control the fuel/air equivalence ratio in the area of the spark plug in order to get a good combustion. This can be achieved in particular through the use of the spray-guided concept and the recently developed piezo-electric injection. Furthermore, optimal geometry design including appropriate piston and bowl shapes are required.

Computational Fluid Dynamics has been used at IFP in the development phase to help in the design and optimization of downsized and/or GDI engines. In particular, the ECFM3Z coherent flame combustion model including an auto-ignition model (TKI) based on tabulated reaction rates allows to correctly simulate the flame propagation for the investigated engine configurations.

The IFP-C3D code is briefly described in the first part of this paper. In a second part, comparisons between numerical results and experimental measurements of spray characteristics in a high pressure cell are presented for both non-evaporating and evaporating conditions. Then, results are shown for a direct injection spark ignition (DISI) engine. Intake stroke, injection and combustion phases are simulated to account for the inhomogeneous distribution of fuel and influence of residual gases on combustion.

CODE DESCRIPTION

Three-dimensional simulations are performed using the multidimensional IFP-C3D code [1] [13]. This code solves the unsteady equations of a chemically reactive mixture of gases, coupled with the equations for a multi-component vaporising fuel spray. The Navier-Stokes equations are solved using a finite volume method extended with the ALE (**A**rbitrary **L**agrangian **E**ulerian) method. The code uses the well known time splitting decomposition. The temporal integration scheme is largely implicit.

Concerning the liquid phase, the physical phenomena of evaporation, break-up using the Wave-FIPA model [6] and spray/wall interaction are included. Collision and coalescence are neglected. In the following simulations, the liquid spray is discretized by the injection of 50,000 computational parcels. Due to the increase of injection pressure for piezo-electric injectors compared to swirl injectors, cavitation can occur inside the nozzle for GDI operating conditions [6]. This can lead to high initial velocity of the spray (up to 200 m/s) that was observed in the experimental visualizations. To improve the prediction of the injection conditions, a strategy similar to that developed for the modeling of transient injection conditions of high pressure Diesel sprays [1] was adopted. In the case of piezo-electric injection, the model accounts for the variations of the injection section during the transient opening and closing phases of the orifice to compute the injection velocity of the liquid particles.

The **A**rk **K**ernel **T**racking **I**gnition **M**odel (AKTIM) [3] [4] is used for spark ignition modelling. For turbulent combustion, the sub-grid description of the 3-**Z**one **E**xtended **C**oherent **F**lame **M**odel (ECFM3Z) developed at IFP is used [2].

The OpenMP paradigm [15] was chosen for parallelization, as it is standardized, portable, scalable, adapted to modern super-scalar SMP machines and has an attractive performance to development cost ratio (easy to implement using only compiler directives).

Profiling of the sequential version allowed to concentrate paralleling efforts on the most CPU time consuming routines: pressure solver, diffusion, matrix inversion (conjugate gradient method with SOR algorithm) and gradient terms (for pressure and Reynolds stress tensor). Overall, about 50 % of the code is parallelised providing a very good and scalable speed-up (around 3 for 4 processors). Details and extensive validations of the code can be found in [13].

HIGH PRESSURE CELL CASES

Simulations of the piezo-electric injection are first conducted in a constant volume cell which enables to study the spray behavior under thermodynamic conditions similar to those of a GDI engine. Calculations are performed in a non uniform cartesian mesh (Figure 1). In the spray region close to the injector (located on the upper face), the cell volume is 1 mm^3 as for typical engine grid spacings. Then it increases up to $\Delta x = \Delta y = \Delta z = 3$ mm in the bottom corners of the high pressure cell.

The injected fuel is iso-octane. Droplets are injected with an initial radius following a Rosin-Rammler distribution with a Sauter Mean Diameter SMR = 7 µm. The injection pressure is 19 MPa and the injection duration is 0.6 ms. From the injection rate (Figure 2) the durations of the opening and closing phases of the injection are estimated to 0.2 ms and 0.1 ms respectively, *i.e.* 50 % of the total duration of the injection.

NON-EVAPORATING CASE

In the first case, injection at room conditions (T_{ch} = 295 K, p_{ch} = 0.12 MPa) is considered.

Figure 3 shows comparisons between experimental visualizations by shadowgraphy and the spray computed with the standard injection model based on the maximum injection section. It appears that the spray penetration velocity is underestimated in this simulation. Accounting for the variations of the injection section during the opening and closing of the orifice leads to an increase of the injection velocity during these transient phases (Figure 4). At the beginning of the injection, the injection rate is low but the injection velocity is already high as the injection section is very small. Then, the injection velocity decreases as the nozzle valve opens before increasing due to the increase of the injection rate. Computing the injection velocity with the maximum injection section leads to an underestimation of the spray momentum during both the opening and closing phases.

Comparisons between the spray computed with the new model and the experimental visualizations are presented in Figure 5. At the end of injection, both the spray shape and penetration are in good agreement with the experiment. This shows the impact of the injection conditions on the spray behavior. Nevertheless, the simulation seems to underpredict the presence of small recirculating droplets at the periphery of the spray. This leads to a smaller spreading of the droplets than in the experiment at t = 1.5 ms. Yet the temporal evolution of the drop SMR on the spray axis is reproduced quite well (Figure 6).

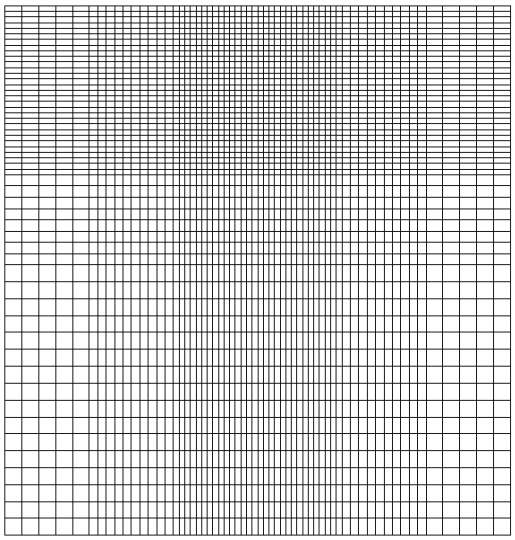

Figure 1: Computational mesh of the high pressure cell (xz plane).

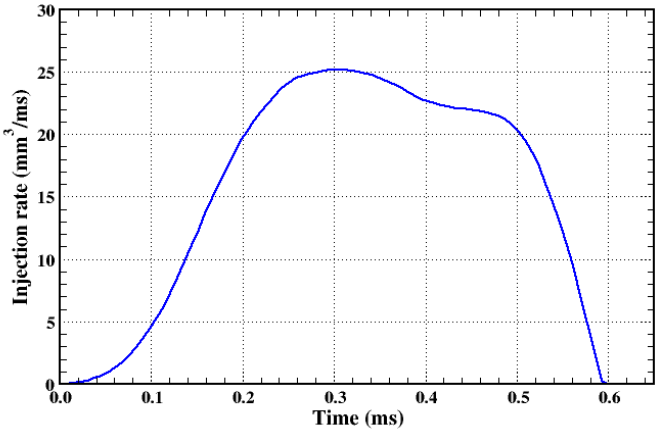

Figure 2: Injection rate in the high pressure cell.

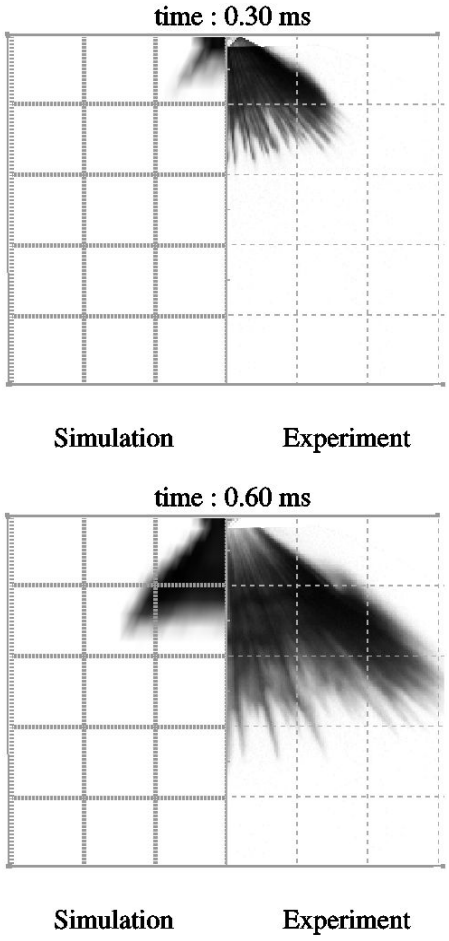

Figure 3: Comparison between experimental visualization and liquid spray computed with the standard injection model (non evaporating case).

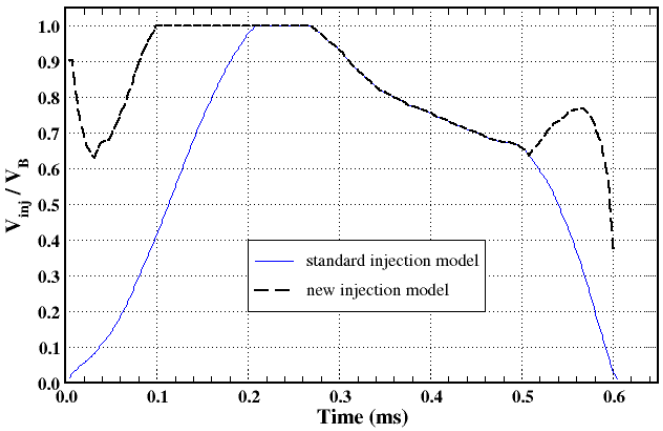

Figure 4: Influence of the transient opening and closing phases on the injection velocity normalized by the Bernoulli velocity V_B.

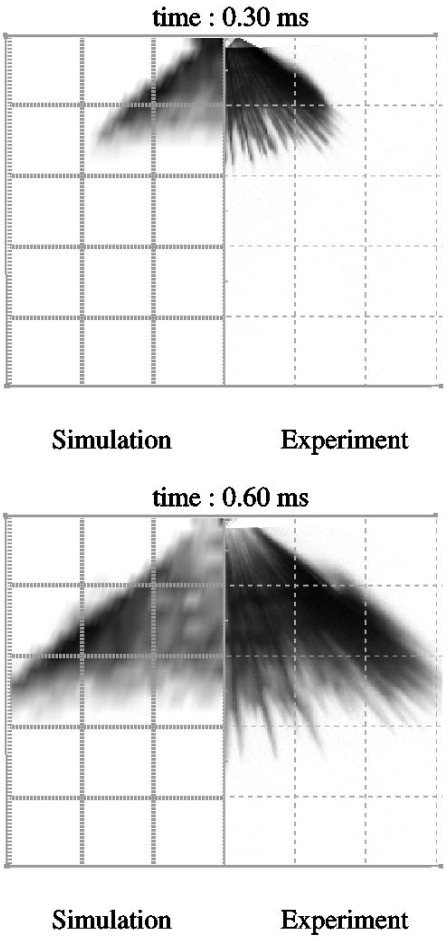

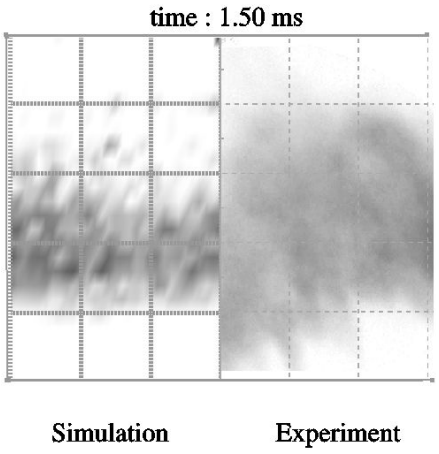

Figure 5: Comparison between experimental visualization and liquid spray computed with the new injection model accounting for transient opening and closing phases (non evaporating case).

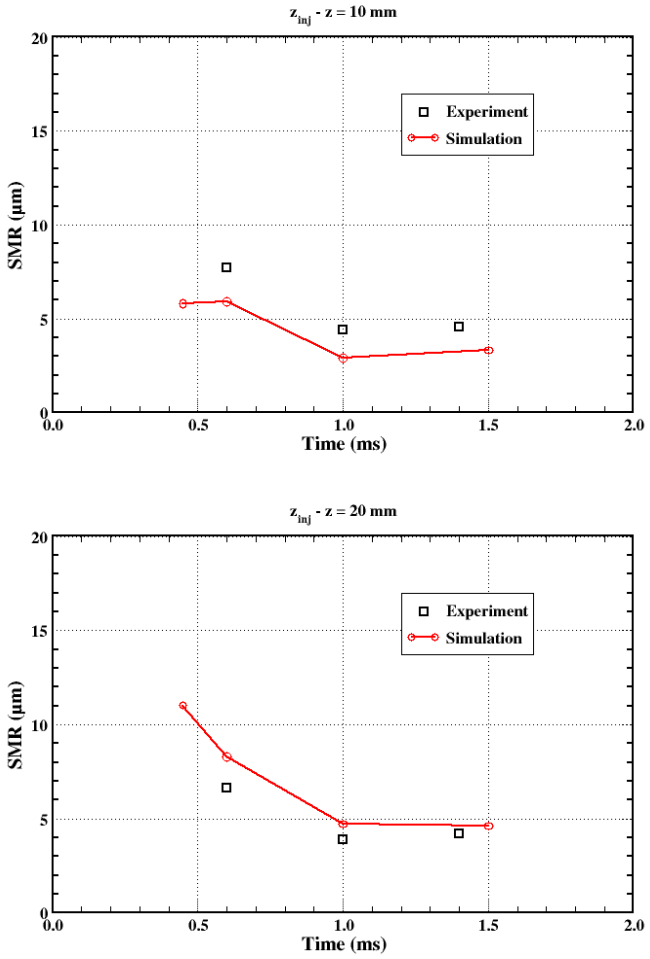

Figure 6: Comparisons between computed and measured SMR on the spray axis (non evaporating case).

EVAPORATING CASE

More recently, ambient evaporating conditions similar to those in a GDI engine were considered (T_{ch} = 455 K, p_{ch} = 0.53 MPa). The injection pressure is 20 MPa and the injection duration is 0.6 ms.

In this case, the liquid phase is observed experimentally in a vertical plane passing through the injector by Laser Induced Exciplex Fluorescence (LIEF). It must be pointed out that the laser plane comes from the left side of the cell. As part of its energy is absorbed during the crossing of the spray, the intensity of the signal coming the right part is more weak, resulting in asymmetric images (Figure 7). For the numerical results, liquid drops are colored by their radius. The spray penetration is fairly well simulated, as well as the recirculation of small drops in the vortex at the tip of the spray.

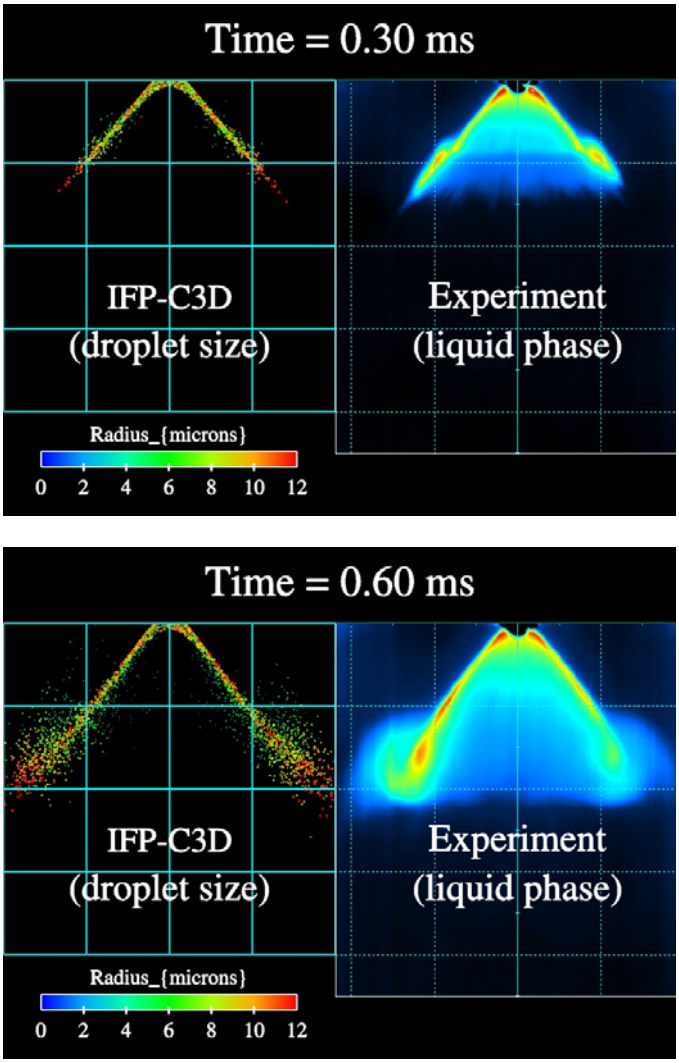

Figure 7: Comparison between computed liquid spray and experimental visualization in a vertical plane passing through the injector (evaporating case).

TURBOCHARGED GDI ENGINE

The use of piezo-electric actuator for injector allows time saving for both opening and closing stages of the injector. As a consequence, the injection duration can be shortened. This allows to better control the fuel location and distribution in the combustion chamber at a given instant in the cycle. Hence, this technology permits to achieve spray guided stratified combustion and make possible combustion with low global fuel/air equivalence ratio. The final targets being a fuel saving and a decrease of pollutant emissions.

The aim of the present case is to test the recently developed models such as the one modeling the piezo-electric injector for an engine configuration. The engine is a DISI single cylinder engine with 500 cm^3 displacement volume for an operating point at 2000 RPM and IMEP = 3.8 bar with a high EGR rate (of around 30%) at intake.

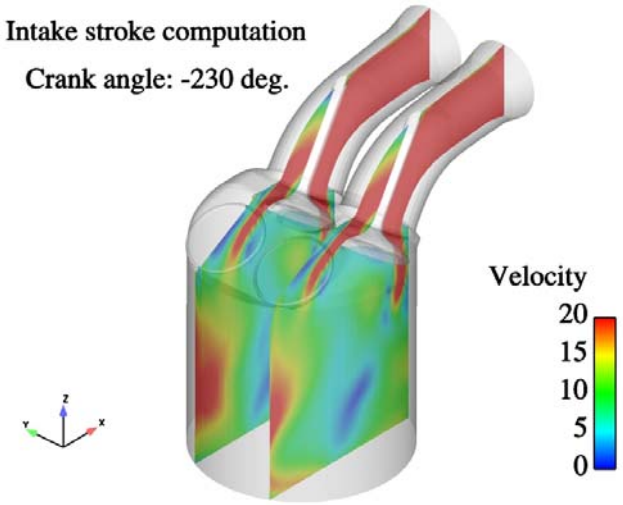

Figure 8: Intake stroke calculation

As it can be observed in Figure 8, fluid motion in the cylinder, trapped mass and in-cylinder composition are results of a previous complete intake stroke computation. At IVC the total residual mass fraction (EGR and burnt gases) is about 38 %. It can be noticed that, in order to simplify the shape of the combustion chamber used for the computation of the intake stroke, the real piston (with bowl) was replaced by a flat one. At the end of this intake computation, the physical quantities are transferred on the mesh representing the real shape of the combustion chamber (see Figure 9) by the use of remapping algorithm.

The mean in-cylinder fuel/air equivalence ratio is 0.5. The piezo-electric injector used was experimentally characterised in a high pressure cell . The injection pressure is 20 MPa. Before performing engine computations, spray parameters (as droplet size and spray cone angle) were obtained by comparing experimental visualizations and measurements in a high pressure cell with calculations under identical operating conditions (as exposed in the paragraph above).

Here computations were carried out using experimental injection and spark timing values.

The computational mesh generated with the software ICEM-CFD (Ansys) is shown in Figure 9. It is composed of mesh cells with sides of about 1.5 mm (previous studies have shown that this cell size is sufficient to get a good level of accuracy). The number of cells in the vertical direction is increased or decreased (as a function of piston position) by use of the remapping algorithm to obtain reasonable aspect ratios. It can be observed that no symmetry assumption is possible due to the piston shape. Moreover the location and the angle of the injector (75° from horizontal) prohibit any symmetry consideration. Consequently, computations were performed on the entire combustion chamber.

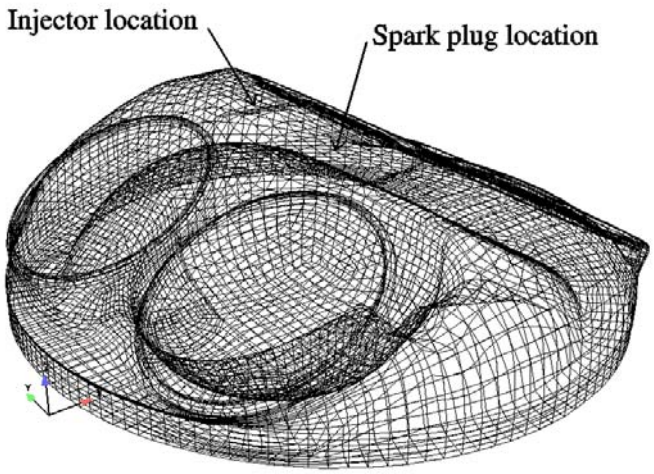

Figure 9: Computational mesh for DISI engine.

The spray location and evolution in the chamber can be compared qualitatively to experimental endoscopic (or other [11]) visualizations. In Figure 10 it can be observed that the penetration and the width evolution of the spray is in good agreement with experimental observations (In this figure one can observe the spark plug representation using the AKTIM model). This allows to deduce that the fuel location and, as a consequence, the fuel/air equivalence ratio in the area of the spark plug is well represented. Hence, the mixing preparation which governs the start and the evolution of the combustion seems to be correctly described.

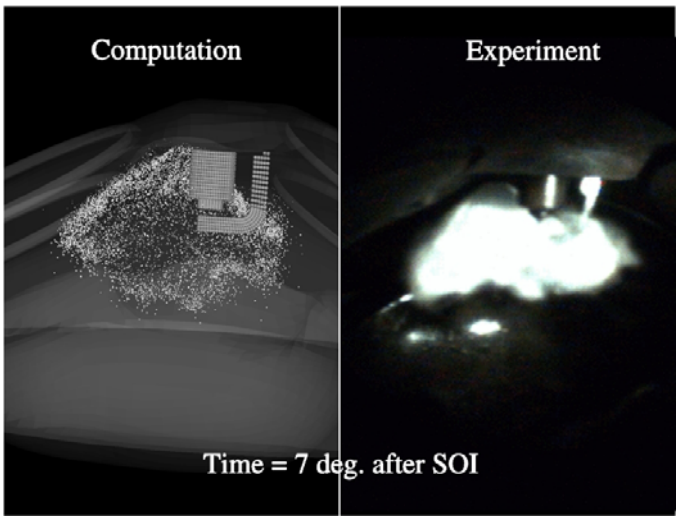

Figure 10: Spray visualization 7 CA deg. after SOI.

The fuel is injected close to the spark plug. Hence, even if the mean fuel/air equivalence ratio is very low, the fuel/air equivalence ratio in the spark plug area is favorable to combustion. This is illustrated in Figure 11 where the distribution of fuel/air equivalence ratio is shown in a vertical plane passing through the spark plug at 7° CA after the start of injection (SOI).

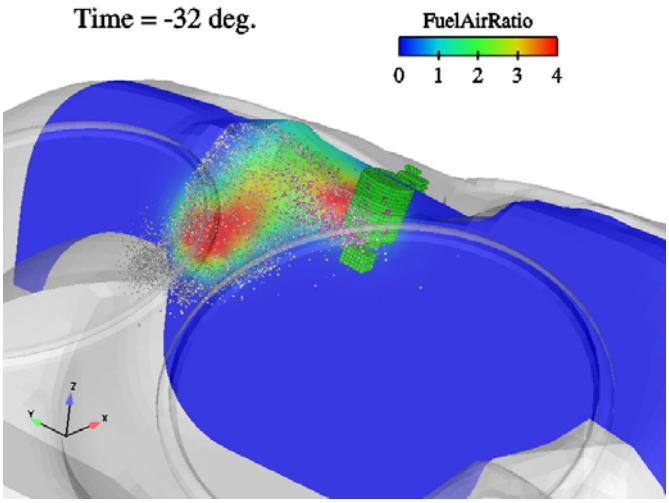

Figure 11: Fuel/air equivalence ratio in a vertical plane passing through the spark plug (7 CA deg. after SOI).

Added to the fact that the fuel/air equivalence ratio is good for the combustion in the area of the spark plug, the injection induces an increase of the turbulence in the combustion chamber which is favorable for the combustion evolution. Even if this increase is mainly located in and around the spray, it can be observed on the mean TKE evolution in Figure 12.

The evolution of the computed in-cylinder pressure compared to the experimental one is given in Figure 13. Computation results are in good agreement with experimental measurements. Moreover, to complete this analysis, the derivative of the numerical pressure can be compared to the experimental one (see Figure 14). It can be observed that the start of combustion, in the computation is a little bit delayed. In spite of that, the general evolution and the extreme values are close to the experimental ones.

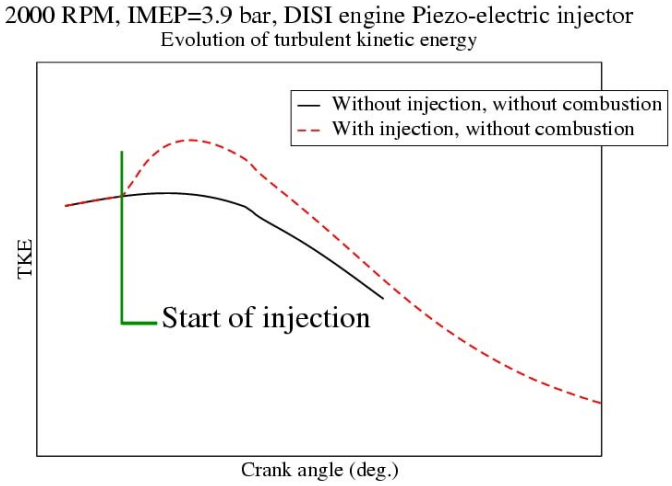

Figure 12: Increase of TKE induced by the spray.

The computed burnt mass fraction (BMF) of fuel reaches its maximum at about 91 % of injected mass. Even if this value is low, it remains close to the experimental one which is equal to 94 %. It may be noticed that this working point is not optimized in terms of SOI and spark advance but was chosen for comparisons with computations because several measurements and pictures of combustion are available. Moreover, even if the numerical pressure remains very close to the measured one, it is slightly underestimated during the expansion stroke. This difference added to the fact that the measured BMF takes into account the end of oxidation occurring during the exhaust stroke, which was not computed, can explain the difference between computation and experiment. The calculated CO_2 emissions are 6.5 % dry and compared well with the experimental value of 7 %.

This kind of computation, taking into account compression, injection and combustion strokes in the whole combustion chamber at low RPM takes about 6 hours on 3 processors (IBM Power4+, 1.7 GHz) of an SMP IBM cluster P655+.

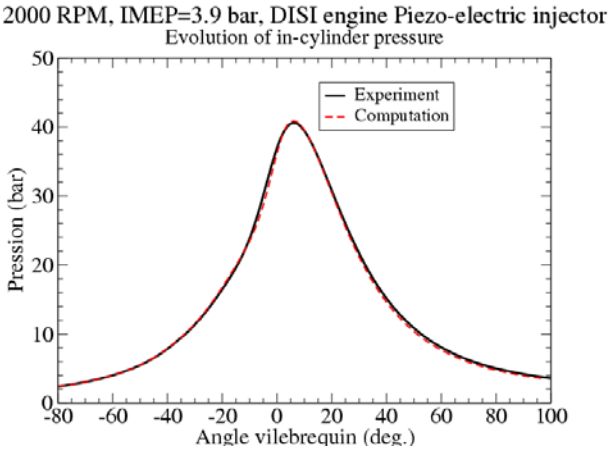

Figure 13: Evolution of in-cylinder pressure.

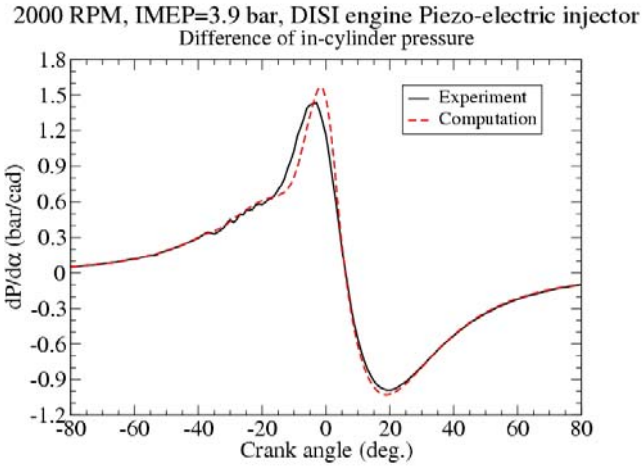

Figure 14: Derivative of in cylinder pressure.

CONCLUSION

This paper presents several results obtained using latest developed injection and combustion models. The numerical modeling of piezo-electric injector was

exposed both in a high pressure cell for non evaporating and evaporating ambient conditions and finally in the case of a DISI engine. It was shown that neglecting the variations of the injection section during both the opening and closing phases of the orifice leads to an important underestimation of the spray momentum and penetration. In all the studied configurations, computed results are in good agreement with the experimental measurements. Even if the final burnt mass fraction is almost equal to 91 % of the injected mass for the DISI engine, the computed in-cylinder pressure evolution remains very close to the experimental one. Moreover, the computation is able to bring new observations and explanation to the combustion of such configuration. Thus, the increase of turbulence due to the spray and the high local fuel/air equivalence ratio are key factors for the combustion evolution for such DISI engine. Further investigations will be carried out for a wider range of operating conditions.

ACKNOWLEDGMENTS

This work was partially supported by GSM (Groupement Scientifique Moteur : Renault, PSA Peugeot-Citroën, IFP). The authors are indebted to P. Pierre (IFP) for his expert technical assistance.

REFERENCES

[1] Béard P., *Towards a predictive modelling of transient injection conditions of Diesel sprays in DID engines*. ILASS Americas, 18th Annual Conference on Liquid Atomization and Spray Systems, Irvine, CA, USA, May 2005.

[2] Colin O. and Benkenida A., *the 3-Zones Extended Coherent Flame Model (ECFM3Z) for computing premixed diffusion combustion*, OGST, Vol. 59, 2004, n°6, pp. 593-609.

[3] Colin O., Pires da Cruz A. and Jay S., *Detailed chemistry-based auto-ignition model including low temperature phenomena applied to 3-D engine calculations*, Proceedings of the Combustion Institute, Vol. 30, pp. 2649-2656, 2005

[4] Duclos J. M. and Colin O., *Arc and Kernel Tracking Ignition Model for 3D Spark Ignition Engine Calculations.* 5th Int. Symp. on Diagnostics and Modeling of Combustion in Internal Combustion Engines, COMODIA 2001, Nagoya, Japan.

[5] Fournet R., Warth V., Glaude P.A., Battin-Leclerc F., Scacchi G., *Automatic Reduction of Detailed Mechanisms of Combustion of Alkanes by Chemical Lumping*, Int. J. Chem. Kinet., Vol. 32, pp. 36-51, 2000.

[6] Gilles-Birth I., Bernhardt S., Spicher U., Rechs M., *A Study of the in-Nozzle Flow Characteristic of Valve Covered Orifice Nozzles for Gasoline Direct Injection*. SAE 2005-01-3684, 2005.

[7] Habchi C., Huynh Huu C., Lambert L., Vanhemelryck J.L., Baritaud T., SAE 970881, 1997.

[8] Henriot S., Bouyssounnouse D., Baritaud T., *Port Fuel Injection and Combustion Simulation of a Racing Engine*. SAE 2003-01-1845, Yokohama, Japan, May 2003.

[9] Heywood J.B. *Internal Combustion Engine Fundamentals***.** McGraw Hill, 1988.

[10] Leduc P., Dubar B., Ranini A., Monnier G., *Downsizing of Gasoline Engine : An Efficient Way to Reduce CO_2 Emissions*. OGST, Vol. 58, 2003, n°1, pp. 115-127.

[11] Smith J.D., Sick V., *Crank-angle Resolved Imaging of fuel Distribution, Ignition and Combustion in a Direct-Injection Spark-Ignition Engine*. SAE 2005-01-3753, 2005.

[12] M. Zolver, A. Benkenida, J. Bohbot, D. Klahr, B. Réveillé, *CFD Tools at IFP for HCCI Engine Simulations*. IMEM Users Group Meeting, Detroit, USA, March 2004.

[13] Zolver M., Klahr D., Bohbot J., Laget O., Torres A., *Reactive CFD in Engines with a New Unstructured Parallel Solver*. OGST, Vol. 58, n°1, pp. 33-46, 2003.

[14] http://www.amesim.com, IMAGINE.

[15] http://www.openmp.org

CONTACT

Dr. P. Béard : Philippe.BEARD@ifp.fr

Dr. O. Laget : Olivier.LAGET@ifp.fr